Cubic lead perovskite PbMoO3 with anomalous metallic behavior

H. Takatsu, O. Hernandez, W. Yoshimune, C. Prestipino, T. Yamamoto, C.
Tassel, Y. Kobayashi, D. Batuk, Y. Shibata, A.M. Abakumov, et al.

Cubic lead perovskite PbMoO$_3$ with anomalous metallic behavior

Hiroshi Takatsu,[1] Olivier Hernandez,[2] Wataru Yoshimune,[1] Carmelo Prestipino,[2] Takafumi Yamamoto,[1] Cedric Tassel,[1] Yoji Kobayashi,[1] Dmitry Batuk,[3] Yuki Shibata,[1] Artem M. Abakumov,[3,4] Craig M. Brown,[5] and Hiroshi Kageyama[1]

[1]*Department of Energy and Hydrocarbon Chemistry, Graduate School of Engineering, Kyoto University, Kyoto 615-8510, Japan*
[2]*Institut des Sciences Chimiques de Rennes, UMR CNRS 6226,*
Université de Rennes 1, Batiment 10B, Campus de Beaulieu, Rennes F-35042, France
[3]*EMAT, University of Antwerp, 2020 Antwerpen, Belgium*
[4]*Skolkovo Institute of Science and Technology, Nobel str. 3, 143026 Moscow, Russia*
[5]*National Institute of Standards and Technology, Center for Neutron Research Gaithersburg, MD 20899-6102, U.S.A.*
(Dated: February 5, 2018)

A previously unreported Pb-based perovskite PbMoO$_3$ is obtained by high-pressure and high-temperature synthesis. This material crystallizes in the $Pm\bar{3}m$ cubic structure at room temperature, making it distinct from typical Pb-based perovskite oxides with a structural distortion. PbMoO$_3$ exhibits a metallic behavior down to 0.1 K with an unusual T-sub linear dependence of the electrical resistivity. Moreover, a large specific heat is observed at low temperatures accompanied by a peak in C_P/T^3 around 10 K, in marked contrast to the isostructural metallic system SrMoO$_3$. These transport and thermal properties for PbMoO$_3$, taking into account anomalously large Pb atomic displacements detected through diffraction experiments, are attributed to a low-energy vibrational mode, associated with incoherent off-centering of lone pair Pb^{2+} cations. We discuss the unusual behavior of the electrical resistivity in terms of a polaron-like conduction, mediated by the strong coupling between conduction electrons and optical phonons of the local low-energy vibrational mode.

PACS numbers: 72.15.-v, 72.80.Ga, 75.40.Cx, 61.05.cf

I. INTRODUCTION

Insulating oxides with a stereochemically active lone pair of Pb^{2+} and Bi^{3+} cations have been the subject of long-standing interest due to large remnant polarization and high temperature structural/electronic transitions, as found in Pb(Zr,Ti)O$_3$ with a coherent displacement of Zr/Ti atoms[1,2]. A surge of interest in multiferroics over the last decade has led to numerous studies of BiFeO$_3$[3] targeting applications in ferroelectric non-volatile memory devices with high working temperature. More recently, there has been a growing attention in ferroelectric-like structural distortion or transition in metallic compounds[4–8]. This is because unprecedented behaviors can appear distinct from conventional metals, such as an enhanced thermoelectric property in (Mo,Nb)Te$_2$[6] and possible odd-parity superconductivity proposed in Cd$_2$Re$_2$O$_7$ and doped SrTiO$_3$ heterostructures[7].

The concept of introducing polar distortion in a metallic phase has been recently demonstrated in a material of the LiNbO$_3$-structure type, LiOsO$_3$[8]. It is discussed that large thermal vibration or incoherent disorder of Li and O ions allows cooperative order upon cooling. A ferroelectric-type structural phase transition occurs at T_s = 140 K, where the metallic conduction associated with Os half-filled t_{2g} states is retained across T_s. In this context, compounds with stereochemically active lone-pair electrons can be considered as an alternative path for designing ferroelectric-like metal or a new class of metal, since the lone pair electrons may promote a certain structural distortion[9,10]. However, the research seeking for novel properties from metallic materials with Pb^{2+} or Bi^{3+} cations is rather limited[11–13].

In this paper, we report the synthesis of a Pb-based perovskite PbMoO$_3$ crystalizing in the cubic structure, despite the presence of Pb^{2+} cations. While this material shows an or-thorhombic distortion with coherent octahedral tiltings at low temperature, it retains a metallic behavior down to 0.1 K. We found an unusual temperature dependence of the electrical resistivity ρ and a large specific heat C_P accompanied by a peak in C_P/T^3. These unusual behaviors are likely originated from a low-energy vibrational mode induced by the incoherent off-centering of lone pair Pb^{2+} cations as suggested from structural refinements. The weak T dependence of ρ is presumably understood in terms of incoherent transport driven by the formation of the polaron-like conduction.

II. EXPERIMENTAL

Polycrystalline samples of Pb$_{1-x}$Sr$_x$MoO$_3$ (x = 0.0, 0.25, 0.5, 0.75), were synthesized by a high-pressure and high-temperature technique. Stoichiometric mixtures of PbO, SrO, and MoO$_2$ were reacted at 1000 °C and 7 GPa for 30 min using a multianvil press. SrMoO$_3$ (x = 1) was synthesized by heating SrMoO$_4$ (prepared by a solid-state reaction) at 1000 °C for 12 h in H$_2$/Ar flow as reported in Ref. 14.

X-ray powder-diffraction (XRD) experiments were performed with Cu $K\alpha$ radiation at room temperature (RT). For an additional structural study of PbMoO$_3$, synchrotron X-ray powder diffraction (SXRD) experiments were performed at RT on the BL02B2 beam line at SPring-8. The wavelength of the incident beam was λ = 0.42089 Å. Neutron diffraction experiments of PbMoO$_3$ were performed at RT and 5 K using the high resolution powder diffractometer BT-1 at the NIST center for Neutron Research. Incident neutrons of wavelength λ = 1.5398 Å monochromated by vertical-focused Cu (311) monochromator was used. The structural refinements were performed using the FullProf and RIETAN-FP softwares[15,16].

The $x = 0$ sample was also characterized using transmission electron microscopy (TEM). The data were acquired on an aberration-corrected FEI Titan 80-300 microscope at 300 kV. The chemical composition was analyzed by an energy dispersive X-ray spectroscopy (EDS). The valence was checked by the X-ray absorption near edge structure (XANES) spectroscopy at the Mo K-edge. The spectra of PbMoO$_3$, SrMoO$_3$, MoO$_2$ and MoO$_3$ were measured at RT on the BL01B1 beamline at SPring-8. The XANES spectra were recorded in a transmittance mode, using Si (111) and Si (311) double crystal monochromator.

The specific heat (C_P) and dc magnetic susceptibility (M/H) were measured, respectively, with a commercial calorimeter (Quantum Design, PPMS) and a SQUID magnetometer (Quantum Design, MPMS). The electrical resistivity ρ was measured by means of a standard four-probe method using rectangular samples cut out from pellets. Gold wires were attached to samples with silver paste, and the samples were then cooled down to 0.1 K using an adiabatic demagnetization refrigerator installed in PPMS. Note that the density of the polycrystalline sample pellet is 8.7 g/cm^3 for PbMoO$_3$, 7.4 g/cm^3 for Pb$_{0.5}$Sr$_{0.5}$MoO$_3$, and 5.4 g/cm^3 for SrMoO$_3$. These values correspond to 89–97% of the calculated ones estimated from the RT crystal structures, suggesting that the difference in density provides only small effect on the absolute values of ρ in these compounds.

III. RESULTS AND DISCUSSION

Figure 1 shows the powder SXRD pattern of PbMoO$_3$ recorded at RT. Observed peaks are indexed in a cubic unit cell, without any splitting and shoulder indicating symmetry lowering (see, for example, 211 and 321 reflections in Figs. 1(b) and 1(c)). This result demonstrates the absence of any distortions from the cubic symmetry at RT. The Rietveld refinement assuming the ideal cubic perovskite (space group: $Pm\bar{3}m$) converged resulting in the lattice parameter of $a = 3.999(1)$ Å and R factors of $R_{wp} = 3.85\%$, $R_e = 3.03\%$, $R_p = 2.99\%$, and $R_B = 3.51\%$. The goodness-of-fit parameter, $S = R_{wp}/R_e$, was $S = 1.27$, indicating excellent quality of the fitting. The solid solution Pb$_{1-x}$Sr$_x$MoO$_3$ was successfully obtained in the entire x range, with the lattice constant decreasing linearly with increasing x (Fig. 1 of the Supplemental Material [17]). These results ensure a continuous change in the A-site composition. Refining the occupancy factor of each atomic site did not improve the overall fit, indicating the stoichiometric composition of the title compound at least for the heavy atoms on the A and B sites. The Mo K-edge XANES spectra of PbMoO$_3$ (Fig. 2), measured together with other Mo compounds, indicate that the formal valence in PbMoO$_3$ is Mo^{4+} (thus yielding Pb^{2+}), which is consistent with the result of bond valence sum calculations based on the RT structure, giving Mo$^{4.08+}$ and Pb$^{1.74+}$. EDS experiments verified the compositional ratio between Pb and Mo, for example, Pb/Mo = 1.01(6) for the $x = 0$ sample.

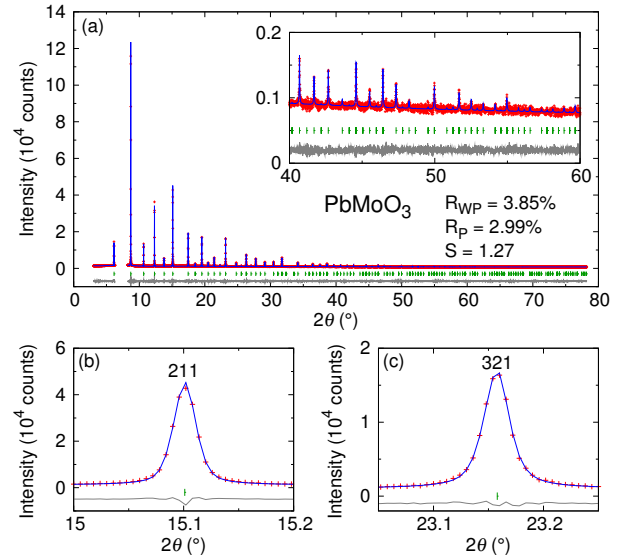Interestingly, a large atomic displacement parameter (ADP) of Pb was obtained (isotropic root-mean-square displacement

FIG. 1. (Color online) (a)Synchrotron patterns of PbMoO$_3$ measured at RT, demonstrating the cubic perovskite structure ($Pm\bar{3}m$). The inset shows the enlarged plot in a high angle region. (b) and (c) are 211 and 321 reflections, respectively, representative peaks with $h \neq k$, $\neq l$, and $l \neq 0$, showing the absence of splitting and shoulder associated with any tetragonal or other symmetry lowering distortions. Observed and refined data are shown by cross and solid curves, and vertical bars represent positions of the Bragg reflections. The difference between the experimental and theoretical data is plotted by the dashed curves at the bottom. Excluded regions in (a) include contributions from small amount of impurities such as PbMoO$_4$.
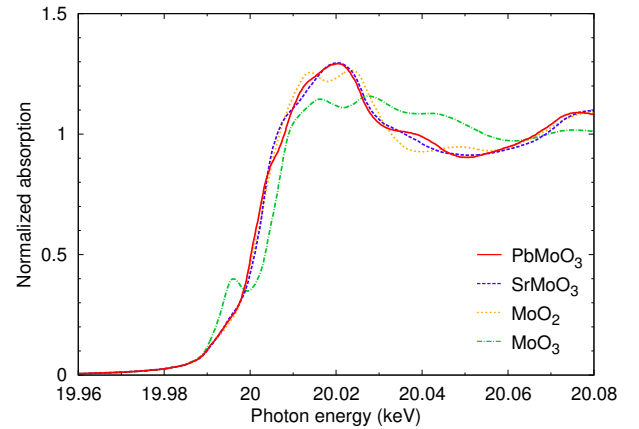

FIG. 2. (Color online) Mo K shell XANES spectra of PbMoO$_3$ (solid line), SrMoO$_3$ (dashed line), MoO$_2$ (dotted line), and MoO$_3$ (dashed dotted line).

of 0.15(1)Å, suggesting unusually large thermal vibration of Pb ions and/or random displacements of Pb away from the ideal position. Given the presence of stereochemically active 6s electrons of Pb^{2+}, the obtained cubic structure in PbMoO$_3$ is unusual and contrasts markedly with other reported Pb-based perovskites with a distortion from the cubic

TABLE I. Structure parameters for PbMoO$_3$ refined by Rietveld analysis of the synchrotron X-ray and neutron diffraction data. For each model, the Mo atom was positioned at the origin. U_{iso} represents the isotropic atomic displacement parameter. Numbers in parentheses indicate one standard deviation in the value.

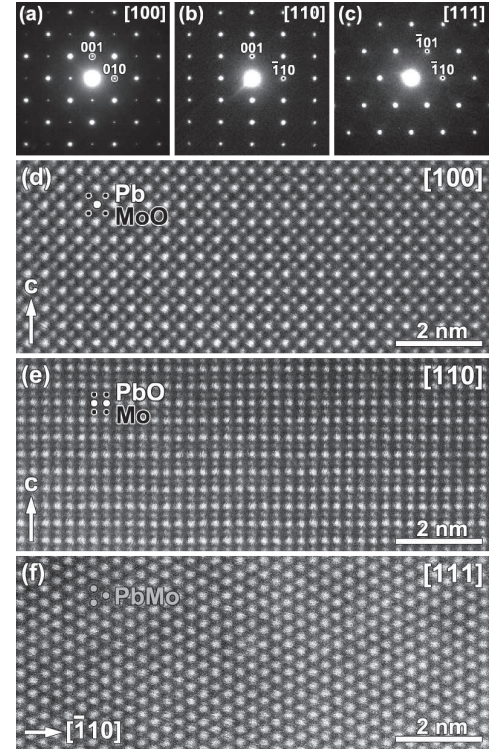|	X-ray (RT)	neutron (RT)	neutron (5 K)
Cell parameters and positions			
Space group	$Pm\bar{3}m$	$Pm\bar{3}m$	$Imma$
a (Å)	3.999(3)	3.9986(1)	5.6348(2)
b (Å)			7.9680(3)
c (Å)			5.6508(2)
Pb x	0.5	0.5	0.0
Pb y	0.5	0.5	0.25
Pb z	0.5	0.5	0.5008(17)
O1 x	0.5	0.5	0.0
O1 y	0.0	0.0	0.25
O1 z	0.0	0.0	0.0259(12)
O2 x			0.25
O2 y			-0.0128(5)
O2 z			0.25
U_{iso} (10^{-2}Å^2)			
Pb	2.08(6)	2.58(5)	1.2(2)
Mo	0.30(6)	0.64(4)	0.36(4)
O1	0.8(3)	0.99(6)	0.6(2)
O2			0.42(8)

FIG. 3. (a)–(c) Electron diffraction patterns and (d)–(f) high resolution HAADF-STEM images of PbMoO$_3$ taken at RT along the [100], [110], and [111] axes. The intensity I in the HAADF-STEM images is proportional to the average atomic number, Z, of the projected atomic column and scales as $I \sim Z^n (n = 1.6 - 1.9)$.

symmetry[13]. In order to gain more insight into the RT crystal structure for PbMoO$_3$, we performed TEM experiments. As shown in Figs. 3(a)–(c), electron diffraction patterns can be consistently indexed on the cubic perovskite structure with the $Pm\bar{3}m$ symmetry. They do not contain any extra reflections or diffuse intensities associated with long or short range ordered structure deformations due to the Pb off-center displacements. Also, high-angle-annular-dark-field scanning-transmission-electron microscopy (HAADF-STEM) images in Figs. 3(d)–(f) do not show any notable discrepancy from the ideal cubic perovskite structure. No anomaly associated with Pb disorder is observed in any principle directions of the cubic structure, [100], [110], and [111]. These results suggest that the Pb off-center displacements, if present, are random at RT, and the local cooperative structure related to correlated disorder[18] or the formation of polar nano region for relaxor phenomena of Pb-based complex perovskites[19–21] is absent.

Rietveld refinement of the RT neutron diffraction data gave a consistent result compared to the SXRD data, confirming the full occupancy of the anionic site, while at T = 5 K we found a orthorhombic distortion with additional peaks corresponding to a $\sqrt{2} \times \sqrt{2} \times 2$ cell (Fig. 2 of the Supplemental Material [17]): a preliminary SXRD experiment shows the structural phase transition appears at $T_s \simeq 200$ K. This superstructure is presumably related to a structural transition as observed in SrMoO$_3$ below 125 K involving the softening

of a R_{25} phonon mode that results in MoO$_6$ octahedral tilting[22]. Indeed, a successful structural refinement at 5 K was conducted assuming a low-temperature structural phase analogous to SrMoO$_3$ (space group: $Imma$): details are given in Tables I and the Supplemental Material [17]. It is notable that, unlike SrMoO$_3$, the displacement parameter of the Pb site is still quite large even at 5 K (root-mean-square displacement of 0.15 Å along the a axis and $\sim$ 0.08 Å along the b and c axes), suggesting a strong "statically" remaining incoherent Pb off-centering. It is worth underlining that the difference in U_{iso} with T for Pb between RT and 5 K is at least three times higher than that for Mo in PbMoO$_3$ or for Sr in SrMoO$_3$[22], additionally revealing an unusual thermal behavior possibly related to the dynamic component of lead disorder. We will discuss the effect of the Pb off-centering on physical properties in the next section. As will be shown below, the absence of any anomalies related to the structural transition in C_P, M/H and ρ may be related to the associated subtle octahedral tilt of about 4° along the a axis.

It is expected that the off-centered Pb^{2+} derived from lone pair electrons in PbMoO$_3$ may provide essential influence on physical properties. In fact, C_P/T of PbMoO$_3$ is much larger than that of SrMoO$_3$ below 150 K. Moreover, the C_P/T^3 vs. T plot for PbMoO$_3$ clearly exhibits a peak centered at about 10 K, which is however absent in SrMoO$_3$ (see the inset of
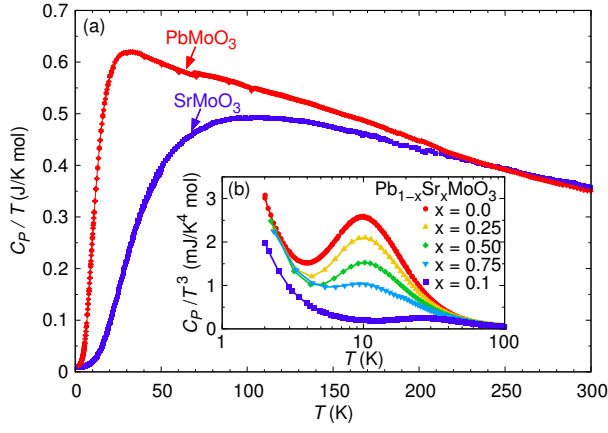
FIG. 4. (Color online) Temperature dependence of C_P/T for powder samples of $PbMoO_3$ and $SrMoO_3$. Large difference of C_P/T emerges below 150 K, suggesting the contribution of a low-energy vibrational mode in $PbMoO_3$. The inset represents the C_P/T^3 vs T plot for $Pb_{1-x}Sr_xMoO_3$.

FIG. 5. (Color online) Temperature dependence of ρ for $PbMoO_3$, $Pb_{0.5}Sr_{0.5}MoO_3$, and $SrMoO_3$. Here the data for $SrMoO_3$ are multiplied by 10 for clarity. A tiny difference of the data at 0 and 0.5 T below 7 K for $PbMoO_3$ is attributed to small amount of a Pb impurity which is less than 0.1% examined from diffraction and magnetic susceptibility experiments. Other signatures of SC transition or spin density wave have not been observed down to 0.1 K in $PbMoO_3$. The inset shows the low-temperature behavior of ρ plotted as a function of $T^{0.5}$ for $PbMoO_3$.

Fig. 4). This low-temperature peak cannot be explained in terms of the structural phase transition of $PbMoO_3$ and the simple Debye law with $C_P(T) \propto T^3$, and hence implies a significant contribution of a low-energy vibrational mode to the specific heat[23,24]. It is also seen that Sr-for-Pb substitution does not alter the C_P/T^3 peak position (temperature), while reducing only its intensity. It can thus be deduced that this peak originates from the incoherent displacement of Pb ions by the $6s$ lone-pair electrons, revealed by the large ADP of Pb, since conventional disorder is known to shift the peak temperature[25–27]. The C_P/T^3 peak for $PbMoO_3$ can be roughly reproduced by the Einstein specific heat with an Einstein temperature $\Theta_E \simeq 50$ K which corresponds to the value estimated from the ADP value of Pb at RT[17]. An upturn of C_P/T^3 observed in $Pb_{1-x}Sr_xMoO_3$ systems below 5 K is ascribed to the electronic specific heat γT, and we obtained $\gamma = 9.2(1)$ mJ/K^2-mol for $PbMoO_3$ and $\gamma = 7.6(1)$ mJ/K^2-mol for $SrMoO_3$, the latter being in agreement with the previous estimation[28,29]. The Wilson ratio $R_W \equiv \pi^2 k_B^2 \chi_0/(3\mu_B^2\gamma)$ is obtained as 1.8 and 2.2 for $PbMoO_3$ and $SrMoO_3$, respectively, using the Pauli paramagnetic susceptibility χ_0 after diamagnetic correction for $PbMoO_3$ and χ_0 from the report on $SrMoO_3$[17,28]. The values of R_W for both compounds are close to 2 as expected in Fermi liquids within the strong correlation limit[30].

Temperature dependence of the electrical resistivity $\rho(T)$ of $PbMoO_3$ (Fig. 5) shows a metallic behavior down to 0.1 K (apart from a tiny contribution of the superconductivity (SC) from the Pb impurity below 7 K). This SC contribution can be removed by applying a magnetic field of 0.5 T, which is above the critical field of the SC transition of Pb. The resulting $\rho(T)$ is almost identical with the zero-field data, implying that the magnetoresistance is negligible. Interestingly, $\rho(T)$ of $PbMoO_3$ exhibits an unusual T-sub linear dependence in a wide temperature range below 100 K, where the fitting with $\rho(T) = A + BT^\alpha$ to the data yielded $\alpha \simeq 0.5$ (the inset of Fig. 5). Moreover, the resistive change in tempera-
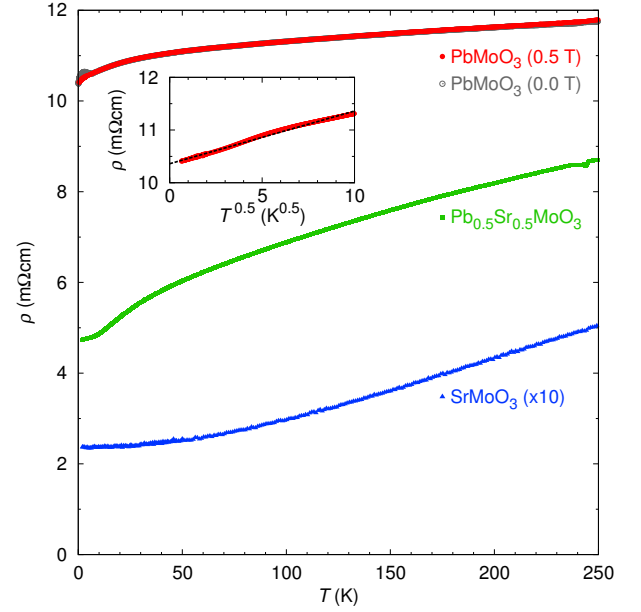
ture is rather small, with a residual resistivity ratio RRR = $\rho(300 \text{ K})/\rho(0.1 \text{ K}) = 1.1$. These features are distinct from $\rho(T)$ of typical non-magnetic metals, where $\rho(T) \propto T$ or $\propto T^5$ due to the electron-phonon scattering with the weak electron-phonon coupling[31,32] and/or $\rho(T) \propto T^2$ due to the electron-electron scattering are observed at low temperature[33,34]. Note that $SrMoO_3$ shows $\rho(T) \propto T^2$ below 140 K (the main panel of Fig. 5) owing to the enhanced electron-electron correlation[29]. We also observed that $\rho(T) \propto T^2$ is recovered by substituting Pb ions by Sr ions at low temperatures for the $x = 0.5$ sample. Therefore, it appears that incoherent off-centered Pb^{2+} ions disturb the electrical conduction. It is known that a weak coupling between optical phonons and conduction electrons gives rise to a T-super linear dependence with $\rho(T) \propto T^n$ ($n \geq 1$)[32,35]. It is thus possible that the observed polaron-like incoherent transport is mediated by strong coupling between conduction electrons and optical phonons of the local low-energy vibrational mode for $PbMoO_3$, as proposed theoretically by Millis et al.[36] It was suggested that $\rho(T) \propto T^{0.5}$ can appear in the critical regime around the crossover from Fermi liquid to polaron behaviors.

IV. CONCLUSION

To summarize, we have synthesized a novel lead perovskite $PbMoO_3$ using a high-pressure and high-temperature reaction. This lead-based compound represents a rare case with the $Pm\bar{3}m$ cubic structure at room temperature, despite the presence of Pb^{2+} cations with lone pair electrons. We observed an unusual T-sub linear dependence in $\rho(T)$ as well as large specific heat at low temperatures, which could be explained in terms of a low-energy vibrational mode mediated by the incoherent off-centering of Pb^{2+} cations as experimentally indicated by anomalously large Pb atomic displacements. Furthermore, the weak T dependence of $\rho(T)$ implies a polaron-like conduction, mediated by the strong trapping of conduction electrons by local phonon vibration.

Note added. Recently, we became aware of the work on $Pb_2Cr_{1+x}Mo_{1-x}O_6$ reporting a synthesis for $x = -1, -2/3, -1/3, 0, 1/3$ ($x = -1$ means $PbMoO_3$), yet with no structural refinement (thus no indication of Pb off-centering) or detailed physical properties[37].

[1] N. Setter and E. L. Cross, *Ferroelectric Ceramics* (Birkhauser Verlag AG, Basel, 1993).

[2] B. Jaffe, W. R. Cook, and H. Jaffe, *Piezoelectric Ceramics* (Elsevier Science & Technology, New York, 1971).

[3] J. Wang, J. B. Neaton, H. Zheng, V. Nagarajan, S. B. Ogale, B. Liu, D. Viehland, V. Vaithyanathan, D. G. S. U. V. Waghmare, N. A. Spaldin, et al., Science **299**, 1719 (2003).

[4] P. W. Anderson and E. I. Blount, Phys. Rev. Lett. **14**, 217 (1965).

[5] I. A. Sergienko, V. Keppens, M. McGuire, R. Jin, J. He, S. H. Curnoe, B. C. Sales, P. Blaha, D. J. Singh, K. Schwarz, et al., Phys. Rev. Lett. **92**, 065501 (2004).

[6] H. Sakai, K. Ikeura, M. S. Bahramy, N. Ogawa, D. Hashizume, J. Fujioka, Y. Tokura, and S. Ishiwata, Sci. Adv. **2**, e1601378 (2016).

[7] V. Kozii and L. Fu, Phys. Rev. Lett. **115**, 207002 (2015).

[8] Y. Shi, Y. Guo, XiaWang, A. J. Princep, D. Khalyavin, P. Manuel, Y. Michiue, A. Sato, K. Tsuda, S. Yu, et al., Nat. Mat. **12**, 1024 (2013).

[9] N. V. Sidgwick, *The Electronic Theory of Valency* (Oxford University Press, UK, 1927).

[10] L. Shimoni-Livny, J. P. Glusker, and C. W. Bock, Inorg. Chem. **37**, 1853 (1998).

[11] S. A. J. Kimber, J. A. Rodgers, H. Wu, C. A. Murray, D. N. Argyriou, A. N. Fitch, D. I. Khomskii, and J. P. Attfield, Phys. Rev. Lett. **102**, 046409 (2009).

[12] J. G. Cheng, J. S. Zhou, and J. B. Goodenough, Phys. Rev.B **80**, 174426 (2009).

[13] J. B. Goodenough and J. Zhou, Sci. Technol. Adv. Mater. **16**, 036003 (2015).

[14] S. Hayashi and R. Aoki, Mat. Res. Bull. **14**, 409 (1979).

[15] J. Rodriguez-Carvajal, Physica B **192**, 55 (1993).

[16] F. Izumi and K. Momma, Solid State Phenom. **130**, 15 (2007).

[17] Supplemental Material of this paper for the powder XRD data of $Pb_{1-x}Sr_xMoO_3$, and for the detailed structure analysis for the neutron diffraction data, and for the analysis of the specific heat and magnetic susceptibility of $PbMoO_3$.

[18] D. A. Keen and A. L. Goodwin, Nature **521**, 303 (2015).

[19] G. Burns and F. H. Dacol, Solid State Commun. **48**, 853 (1983).

[20] S. B. Vakhrushev, B. E. Kvyatkovsky, A. A. Naberezhnov, N. M. Okuneva, and B. P. Toperverg, Ferroelectrics **90**, 173 (1989).

[21] K. Hirota, Z. G. Ye, S. Wakimoto, P. M. Gehring, and G. Shirane, Phys Rev B **65**, 104105 (2002).

[22] R. B. Macquart, B. J. Kennedy, and M. Avdeev, J Solid State Chem. **183**, 249 (2010).

[23] A. P. Ramirez and G. R. Kowach, Phys. Rev. Lett. **80**, 4903 (1998).

[24] T. H. K. Barron and G. K. White, *Heat Capacity and Thermal Expansion at Low Temperatures* (Springer, New York, 1999).

[25] R. O. Pohl and E. T. Swartz, J. Non-Cryst. Solids **76**, 117 (1985).

[26] D. J. Safarik, R. B. Schwarz, and M. F. Hundley, Phys. Rev. Lett. **96**, 195902 (2006).

[27] B. C. Melot, R. Tackett, J. O'Brien, A. L. Hector, G. Lawes, R. Seshadri, and A. P. Ramirez, Phys. Rev. B **79**, 224111 (2009).

[28] S. Ikeda and N. Shirakawa, Physica C **341**, 785 (2000).

[29] I. Nagai, N. Shirakawa, S. Ikeda, R. Iwasaki, H. Nishimura, and M. Kosaka, Applied Physics Letters **87**, 024105 (2005).

[30] H. Kronmüller and S. Parkin, *Handbook of Magnetism and Advanced Magnetic Materials* (Wiley-Interscience, USA, 2007).

[31] J. M. Ziman, *Electrons and Phonons* (Oxford University Press, New York, 1960).

[32] P. B. Allen and W. W. Schulz, Phys. Rev. B **47**, 14434 (1993).

[33] A. P. Mackenzie and Y. Maeno, Rev. Mod. Phys. **75**, 657 (2003).

[34] K. Kadowaki and S. B. Woods, Solid State Commun. **58**, 507 (1986).

[35] T. Masui, K. Yoshida, S. Lee, A. Yamamoto, and S. Tajima, Phys. Rev. B **65**, 214513 (2002).

[36] A. J. Millis, R. Mueller, and B. I. Shraiman, Phys. Rev. B **54**, 5389 (1996).

[37] H. F. Zhao, L. P. Cao, Y. J. Song, S. M. Feng, X. Shen, X. D. Ni, Y. Yao, Y. G. Wang, R. M. Wang, C. Q. Jin, et al., J. Solid. State Chem. **246**, 92 (2017).

Supplemental Material: Cubic lead perovskite PbMoO$_3$ with anomalous metallic behavior

I. ABSTRACT

In this supplemental material, we describe the synthesis of solid solutions of Pb$_{1-x}$Sr$_x$MoO$_3$ ($x = 0.0, 0.25, 0.5, 0.75, 1.0$) with these powder X-ray diffraction (XRD) data. We also show the result of neutron diffraction measurements and the analysis of the specific heat C_P as well as the result of magnetic susceptibility M/H for the $x = 0$ sample of PbMoO$_3$.

II. SYNTHESIS OF PB$_{1-x}$SR$_x$MOO$_3$

Samples of Pb$_{1-x}$Sr$_x$MoO$_3$ were obtained by the same method for the synthesis of PbMoO$_3$. XRD patterns of these samples obtained through a laboratory X-ray machine at room temperature (RT) represent the same pattern of PbMoO$_3$ (Fig. S1), indicating that the samples crystalize into the cubic structure in the entire x range. The estimated lattice parameters linearly decrease with increasing x (the inset of Fig. S1), which ensures the stoichiometric mixture of the samples. It is observed that impurity peaks such as PbMoO$_4$ and Pb appear in the XRD patterns, however those concentrations are estimated to be small enough ($< 1\%$).
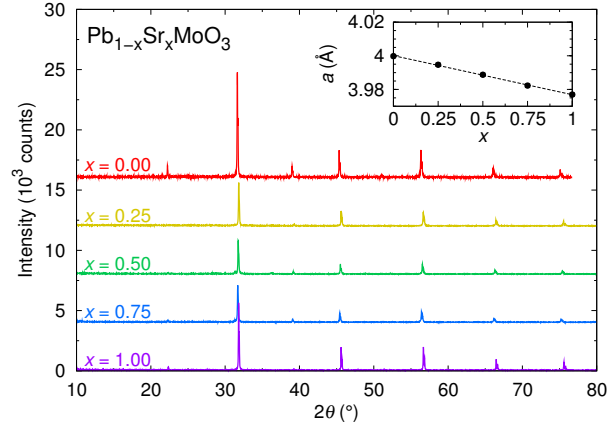

FIG. S1. (Color online) XRD patterns of Pb$_{1-x}$Sr$_x$MoO$_3$ ($x = 0.0, 0.25, 0.5, 0.75, 1.0$) at RT. Inset is the lattice parameter a plotted as a function of x.

Neutron diffraction measurements on the $x = 0$ sample at 5 K show an additional peak or splitting of peaks from the $Pm\bar{3}m$ cubic symmetry observed at RT (e.g., around 70° in Fig. S2). These peaks are not magnetic in the origin, because magnetic susceptibility experiments did not show any signature of magnetic phase transition. We therefore analyzed the low-temperature crystal structure, assuming the $Imma$ structure which is the orthorhombic space group (SG) of the highest symmetry: this choice is reasonable because other orthorhombic SGs of lower symmetry, fulfilling the observed I-centering, such as $Immm$, $Ibam$, $Ibca$, $Imm2$, $Iba2$, $Ima2$, $I222$, and $I2_12_12_1$ are incompatible with the extinction conditions. We also reexamined the RT $Pm\bar{3}m$ structural model of the synchrotron XRD analysis by the Rietveld refinement against neutron data. The resulting curves are shown in Fig. S2, and the obtained structural parameters are presented in Table I of the main text. The R factors of the Rietveld refinement are $R_{wp} = 16.3\%$, $R_e = 17.8\%$, $R_p = 19.2\%$, $R_B = 2.28\%$ for RT, and $R_{wp} = 15.9\%$, $R_e = 16.9\%$, $R_p = 16.2\%$, $R_B = 2.56\%$ for 5 K. The goodness-of-fit parameter, $S = R_{wp}/R_e$, was $S = 0.915$ and 0.940 for RT and 5 K, indicating excellent quality of fittings.

The key feature of the low temperature $Imma$ structe in PbMoO$_3$ lies in the elongated shape of the Pb anisotropic displacement parameters along the a axis that corresponds to the [101] direction of the high temperature cubic unit cell (Fig. S3). This result is also supported by using difference Fourier syntheses and maximum entropy method (MEM) calculations. These analyses clarify that the Pb nuclear density is homogeneously elongated along the a axis without any maximum density on each side of the $4e$ Wyckoff site.
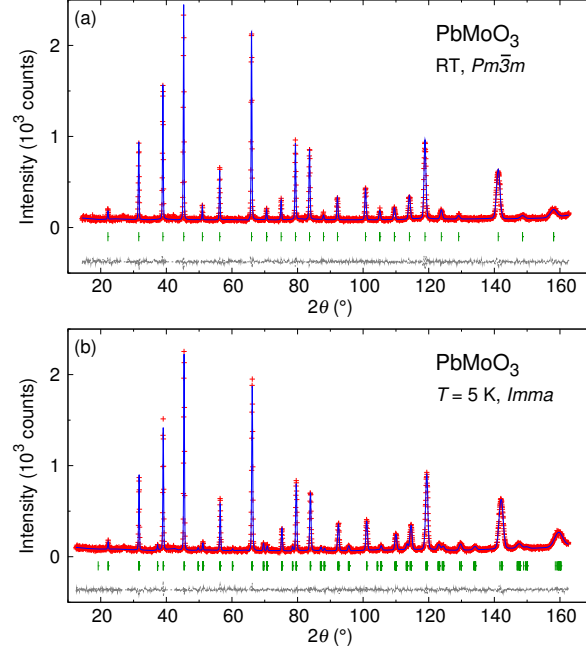
FIG. S2. (Color online) Neutron diffraction patterns of PbMoO₃ measured at (a) RT and (b) 5 K. Observed and refined data are shown by cross and solid curves, respectively, and vertical bars represent positions of the Bragg reflections. The difference between the experimental and theoretical data is plotted by the dashed curves at the bottom.
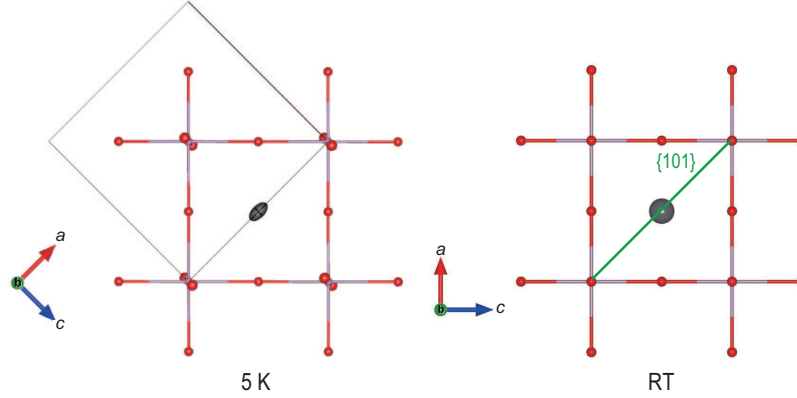

FIG. S3. (Color online) Crystal structures of PbMoO₃ at 5 K (left) and RT (right), featuring the Pb environment. Gray ellipsoid or sphere represent the Pb ion drawn with the anisotropic displacement parameters. Red and purple spheres represent O and Mo ions, respectively. A squre lattice, shown by gray lines in the left, represents the unit cell of the *Imma* structure.

III.   ANALYSIS OF SPECIFIC HEAT

In order to analyze the anomalous behavior of the $C_P(T)/T^3$ peak observed in PbMoO₃, we have fitted the data as follows.

The phonon contribution to the low temperature specific heat, $C_{\mathrm{ph}}(T)$, can be modeled as a sum of Debye and Einstein terms[S1,S2], $C_{\mathrm{D},i}(T)$ and $C_{\mathrm{E},j}(T)$ [$i = 1, 2, ...; j = 1, 2, ...$], i.e.,

$$C_{\mathrm{ph}}(T) = \sum_i f_{\mathrm{D},i} C_{\mathrm{D},i}(T) + \sum_j f_{\mathrm{E},j} C_{\mathrm{E},j}(T), \tag{S1}$$

where $f_{\mathrm{D},i}$ and $f_{\mathrm{E},j}$ are fitting parameters representing the number of the Debye and Einstein modes for the i- and j-th contributions. The sum of these coefficients represents the total number of lattice dynamical modes in the unit cell, i.e.,
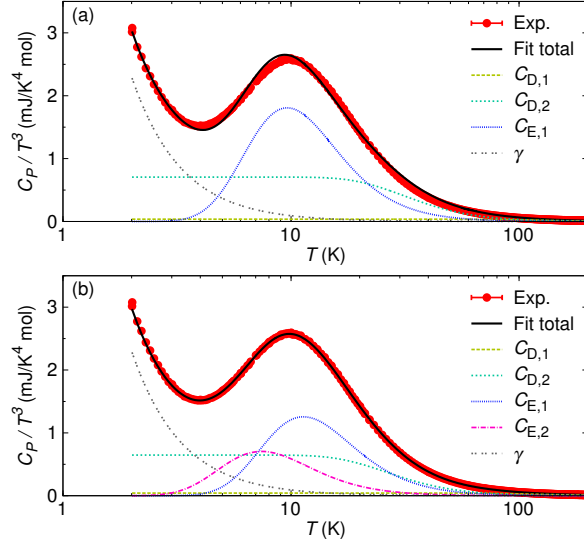
FIG. S4. (Color online) Results of fitting of the specific heat data shown in the inset of Fig. 4 of the main text. In (a), two Debye and one Einstein terms were used for the fitting with Eq. (S4), while in (b), two Debye and two Einstein terms were used.

TABLE I. Parameters obtained by fitting of the specific heat data for PbMoO$_3$. Here, the Debye and Einstein modes of Eq. (S1) are represented as Di ($i = 1, 2$) and Ej ($j = 1, 2$), respectively.

Two Debye and one Einstein model [Fig. S4(a)]		
Mode	$\Theta_{\mathrm{D},i}$, $\Theta_{\mathrm{E},j}$ (K)	$f_{\mathrm{D},i}$, $f_{\mathrm{E},j}$
D1	560	9.92
D2	154	3.99
E1	47.4	1.09

Two Debye and two Einstein model [Fig. S4(b)]		
Mode	$\Theta_{\mathrm{D},i}$, $\Theta_{\mathrm{E},j}$ (K)	$f_{\mathrm{D},i}$, $f_{\mathrm{E},j}$
D1	560	11.4
D2	129	2.15
E1	55.9	1.23
E2	36.9	0.19

$\sum_i f_{\mathrm{D},i} + \sum_j f_{\mathrm{E},j} = 15$ for PbMoO$_3$. $C_{\mathrm{D},i}(T)$ and $C_{\mathrm{E},j}(T)$ represent the contribution of Debye phonons and Einstein phonons to the specific heat, expressed as

$$C_{\mathrm{D},i}(T) = 3\,R\Big(\frac{T}{\Theta_{\mathrm{D},i}}\Big)^3 \int_0^{\Theta_{\mathrm{D},i}/T} \frac{e^x x^4\,dx}{(e^x - 1)^2}, \tag{S2}$$

$$C_{\mathrm{E},j}(T) = R\,\frac{e^{\Theta_{\mathrm{E},j}/T}}{(e^{\Theta_{\mathrm{E},j}/T} - 1)^2}\Big(\frac{\Theta_{\mathrm{E},j}}{T}\Big)^2, \tag{S3}$$

where R is the gas constant, and $\Theta_{\mathrm{D},i}$ and $\Theta_{\mathrm{E},j}$ are fitting parameters representing Debye and Einstein temperatures, respectively. We tentatively used these formulations for the specific heat analysis for PbMoO$_3$, in reference to other systems[S3–S7,S23,S24].

The least-squares fitting was carried out using the data between 2 and 100 K, and the relation

$$C_P(T) = \gamma T + C_{\mathrm{ph}}(T), \tag{S4}$$

with taking into account the electronic specific heat constant $\gamma = 9.2(1)$ mJ/K^4 mol for PbMoO$_3$. In the primary fit, we considered two Debye and one Einstein modes ($i = 2$, $j = 1$) and obtained reasonable fitting results reproducing experimental features as

shown in Fig S4(a). It is seen that the C_P/T^3 peak is reproduced by the Einstein specific heat with $\Theta_{E,1} \simeq 50$ K. This value agrees well with the estimation of the Einstein temperature $\Theta_E = 58$ K from the isotropic atomic displacement parameter U_{iso} of Pb at RT for the relation between U_{iso} and $\Theta_E{}^{S8}$, i.e., $U_{iso} = h^2T/4\pi mk_B\Theta_E^2$, where h and k_B are the Planck and Boltzmann constants, respectively, and m is the atomic mass. This implies the close relation between the local vibrational mode mediated by incoherent off-centered Pb^{2+} cations and large low-temperature specific heat featured by the C_P/T^3 peak at about 10 K. The obtained fitting parameters are listed in Table I. Note that the high-temperature part from one Debye contribution with $\Theta_{D,1} = 560$ K provides a reasonable value for high-temperature mode in oxides which mainly contributes to the data for $T > 100$ K. It is worth noting that the model with two Debye and two Einstein modes can slightly improve the fitting as shown in Fig. S4(b), and the obtained fitting parameters are listed in Table I. This result suggests that a low-energy optical mode of $PbMoO_3$ is weakly dispersive.

IV. MAGNETIC SUSCEPTIBILITY OF PBMOO$_3$

The temperature dependence of M/H of $PbMoO_3$ measured at $H = 1000$ Oe does not show any signature of the phase transition and hysteresis between zero-field cooling and field cooling runs (Fig. S5). A tiny diamagnetic signal accompanied by the superconducting transition of Pb impurities was observed in low field below 7 K, however its amount is less than 1% in our samples. Note that in particular, the estimated impurity amount for the sample used in the resistivity measurements is less than 0.1%. In accordance with a slight enhancement of Pauli paramagnetic susceptibility, M/H of $PbMoO_3$ is T-independent in a wide temperature range above 20 K, while the Curie-type increase below 20 K corresponds to small amount (about 0.1%) of free impurity spins. The Pauli paramagnetic susceptibility is estimated as $\chi_0 = 2.2 \times 10^{-4}$ emu/mol after the correction of the diamagnetic susceptibility of $\chi_{dia} = -8.1 \times 10^{-5}$ emu/mol. This value of χ_0 is similar to the value reported in $SrMoO_3{}^{S9-S11}$.
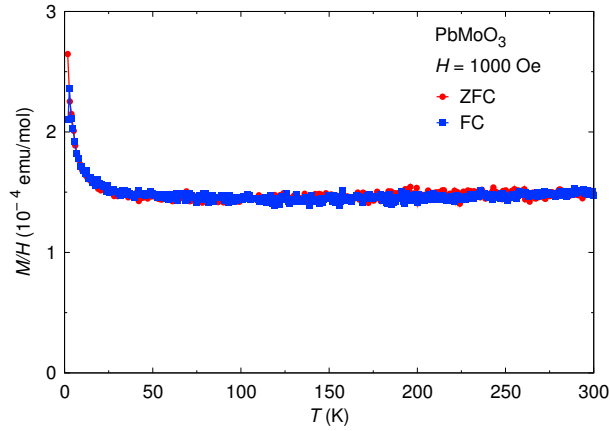

FIG. S5. (Color online) Temperature dependence of the magnetic susceptibility M/H of the polycrystalline sample of $PbMoO_3$ at $H = 1000$ Oe. Note, 1 emu = 10^{-3} A m^2.

[S1] A. P. Ramirez and G. R. Kowach, Phys. Rev. Lett. **80**, 4903 (1998).
[S2] T. H. K. Barron and G. K. White, *Heat Capacity and Thermal Expansion at Low Temperatures* (Springer, New York, 1999).
[S3] V. Keppens, D. Mandrus, B. C. Sales, B. C. Chakoumakos, P. Dai, R. Coldea, M. B. Maple, D. A. Gajewski, E. J. Freeman, and S. Bennington, Nature **395**, 876 (1998).
[S4] Y. Yamamura, N. Nakajima, T. Tsuji, Y. Iwasa, K. Saito, and M. Sorai, Solid State Commun. **121**, 213 (2002).
[S5] M. Tachibana, K. Sasame, H. Kawaji, T. Atake, and E. Takayama-Muromachi, Phys. Rev. B **80**, 094115 (2009).
[S6] B. C. Melot, R. Tackett, J. O'Brien, A. L. Hector, G. Lawes, R. Seshadri, and A. P. Ramirez, Phys. Rev. B **79**, 224111 (2009).
[S7] H. Takatsu, S. Yonezawa, S. Mouri, S. Nakatsuji, K. Tanaka, and Y. Maeno, J. Phys. Soc. Jpn. **76**, 104701 (2007).
[S8] T. M. Tritt, *Recent Trends in Thermoelectric Materials Research, Part Two, Semiconductors and Semimetals, Volume 70* (Academic Press, New York, 2000).
[S9] S. Ikeda and N. Shirakawa, Physica C **341**, 785 (2000).
[S10] S. B. Zhang, Y. P. Sun, B. C. Zhao, X. B. Zhu, and W. H. Song, Solid State Commun. **138**, 123 (2006).
[S11] B. C. Zhao, Y. P. Sun, S. B. Zhang, W. H. Song, and J. M. Dai, J. Appl. Phys. **102**, 113903 (2007).